Monthly Notices
of the
ROYAL ASTRONOMICAL SOCIETY

MNRAS **438,** 3521–3534 (2014)
Advance Access publication 2014 January 24

doi:10.1093/mnras/stt2464

Multiwavelength observations of the γ-ray-emitting narrow-line Seyfert 1 PMN J0948+0022 in 2011

F. D'Ammando,[1,2]★ J. Larsson,[3] M. Orienti,[1,4] C. M. Raiteri,[5] E. Angelakis,[6] A. Carramiñana,[7] L. Carrasco,[7] A. J. Drake,[8] L. Fuhrmann,[6] M. Giroletti,[1] T. Hovatta,[9] W. Max-Moerbeck,[9] A. Porras,[7] A. C. S. Readhead,[9] E. Recillas[7] and J. L. Richards[10]

[1]*INAF – Istituto di Radioastronomia, Via Gobetti 101, I-40129 Bologna, Italy*
[2]*Dipartimento di Fisica, Università degli Studi di Perugia, Via A. Pascoli, I-06123 Perugia, Italy*
[3]*KTH, Department of Physics, and the Oskar Klein Centre, AlbaNova, SE-106 91 Stockholm, Sweden*
[4]*Dipartimento di Astronomia, Università di Bologna, Via Ranzani 1, I-40127 Bologna, Italy*
[5]*INAF – Osservatorio Astrofisico di Torino, Via Osservatorio 20, I-10025 Pino Torinese (TO), Italy*
[6]*Max-Planck-Institute für Radioastronomie, Auf dem Hügel 69, D-53121 Bonn, Germany*
[7]*Instituto National de Astrofísica, Óptical, y Electrónica, Tonantzintla, 72840 Puebla, Mexico*
[8]*California Institute of Technology, 1200 E. California Blvd, CA 91225, USA*
[9]*Cahill Center for Astronomy and Astrophysics, California Institute of Technology 1200 E. California Blvd, Pasadena, CA 91125, USA*
[10]*Department of Physics, Purdue University, 525 Northwestern Avenue, West Lafayette, IN 47907, USA*

Accepted 2013 December 19. Received 2013 November 27; in original form 2013 October 3

ABSTRACT

We report on radio-to-γ-ray observations during 2011 May–September of PMN J0948+0022, the first narrow-line Seyfert 1 (NLSy1) galaxy detected in γ-rays by *Fermi*-Large Area Telescope. Strong variability was observed in γ-rays, with two flaring periods peaking on 2011 June 20 and July 28. The variability observed in optical and near-infrared seems to have no counterpart in γ-rays. This different behaviour could be related to a bending and inhomogeneous jet or a turbulent extreme multicell scenario. The radio spectra showed a variability pattern typical of relativistic jets. The *XMM* spectrum shows that the emission from the jet dominates above ∼2 keV, while a soft X-ray excess is evident in the low-energy part of the X-ray spectrum. Models where the soft emission is partly produced by blurred reflection or Comptonization of the thermal disc emission provide good fits to the data. The X-ray spectral slope is similar to that found in radio-quiet NLSy1, suggesting that a standard accretion disc is present, as expected from the high accretion rate. Except for the soft X-ray excess, unusual in jet-dominated active galactic nuclei, PMN J0948+0022, shows all characteristics of the blazar class.

Key words: galaxies: active – galaxies: individual: (PMN J0948+0022) – galaxies: nuclei – galaxies: Seyfert – gamma-rays: galaxies – gamma-rays: general.

1 INTRODUCTION

Narrow-line Seyfert 1 (NLSy1) galaxies, first suggested as a distinct class of active galactic nuclei (AGNs) by Osterbrock & Pogge (1985), are characterized in optical by their narrow permitted emission lines (full width at half-maximum, FWHM $\leq$ 2000 km s^{-1}), weak [O III]λ5007 emission line ([O III]/Hβ < 3) and strong Fe II emission lines. They also exhibit strong X-ray variability, steep X-ray spectra, substantial soft X-ray excess and relatively high luminosity (Boller, Bradt & Fink 1996; Zhou et al. 2006). These characteristics suggest that NLSy1s have smaller masses of the central black hole (BH; $M_{\rm BH} = 10^6$–10^8 M$_\odot$) and higher $\dot{M}/\dot{M}_{\rm Edd}$ values (up to the Eddington limit or above) than those observed in blazars and radio galaxies. Only a small percentage (<7 per cent) of NLSy1 are radio loud (Komossa et al. 2006) compared to ∼15 per cent of the quasars. In the radio-loud NLSy1s, flat radio spectra and flux density variability suggest that several of them could host relativistic jets (Zhou et al. 2003; Doi et al. 2006; Yuan et al. 2008).

PMN J0948+0022 shows optical properties typical of an NLSy1 [i.e. FWHM (Hβ) = 1432 ± 87 km s^{-1}, [O III]/Hβ ∼0.1, a strong Fe II bump] and a radio loudness of R = 355 (Yuan et al. 2008). High brightness temperature and a compact structure have been

★ E-mail: dammando@ira.inaf.it

observed for PMN J0948+0022 (Doi et al. 2006), in addition to a possible core–jet structure (Giroletti et al. 2011). This source was the first radio-loud NLSy1 to be detected in γ-rays by the Large Area Telescope (LAT) on board the *Fermi Gamma-ray Space Telescope* (Abdo et al. 2009a). After that, other four radio-loud NLSy1s were detected with high significance in γ-rays (Abdo et al. 2009b; D'Ammando et al. 2012a), suggesting the radio-loud NLSy1s as a third class of γ-ray-emitting AGN with relativistic jets. In contrast, no radio-quiet Seyfert galaxies have been detected in γ-rays (Ackermann et al. 2012). Three γ-ray flares were observed from PMN J0948+0022 during 2010–2013, reaching daily peak fluxes of (1–2) $\times$ 10^{-6} photons cm^{-2} s^{-1} (D'Ammando & Ciprini 2011; Foschini et al. 2011; D'Ammando & Orienti 2013). This indicates that radio-loud NLSy1s also can host powerful relativistic jets such as blazars. These findings pose intriguing questions about the nature of these γ-ray-emitting NLSy1s, the onset of production of their relativistic jets and the cosmological evolution of radio-loud AGNs.

After the discovery of γ-ray emission from PMN J0948+0022, this source has been the target of different multifrequency campaigns with the aim of understanding its nature. The first spectral energy distributions (SEDs) collected for this object, as well as for the other three γ-ray NLSy1s detected in the first year of *Fermi* operation, showed clear similarities with blazars: a double-humped shape with a first peak in the IR/optical band due to synchrotron emission, a second peak in the MeV/GeV band likely due to inverse Compton emission and an accretion disc component in UV. The physical parameters of these NLSy1s are blazar like, and jet powers are in the average range of blazars (Abdo et al. 2009b). In addition, the comparison of the SED of PMN J0948+0022 during the 2010 July flaring activity with that of 3C 273, a typical flat spectrum radio quasar (FSRQ), showed a more extreme Compton dominance in the NLSy1. The disagreement between the two SEDs can be due to the difference in BH masses and Doppler factor of the two jets (Foschini et al. 2011). The radio-to-γ-ray light curves of the source collected over years showed correlated variability, with a delay of a few months of the radio emission with respect to the gamma-rays, as usually observed in FSRQs (Abdo et al. 2009c; Foschini et al. 2012).

In this paper, we discuss the results of the analysis of the multiwavelength data of PMN J0948+0022 collected during 2011 May–September. Part of the data presented here has been already published in Foschini et al. (2012). *XMM–Newton* and Catalina Real-time Transient Survey (CRTS) data are presented here for the first time. *Fermi*-LAT, *Swift* and MOJAVE data are re-analysed. This paper is organized as follows. In Section 2, we report the LAT data analysis and results, while in Sections 3 and 4, we present the X-ray and optical/UV results of the *Swift* and *XMM–Newton* observations, respectively. Near-infrared (NIR) and optical data from ground-based observatories are presented and discussed in Section 5. Radio data collected by the very long baseline array (VLBA) interferometer, the 40 m Owens Valley Radio Observatory (OVRO), the 32 m Medicina, the 13.7 m Metsähovi and 100 m Effelsberg single-dish telescopes are presented and discussed in Section 6. In Section 7, we discuss the properties of the source and draw our conclusions.

Throughout this paper, the quoted uncertainties are given at the 1σ level, unless otherwise stated, and the photon indices are parametrized as $\mathrm{d}N/\mathrm{d}E \propto E^{-\Gamma}$, where Γ is the photon index. We adopt a Λ cold dark matter cosmology with $H_0 = 71$ km s^{-1} mpc^{-1}, $\Omega_\Lambda = 0.73$ and $\Omega_\mathrm{m} = 0.27$. The corresponding luminosity distance at $z = 0.5846$ is $d_\mathrm{L} = 3413$ Mpc, and 1 arcsec corresponds to a projected size of 6.590 kpc.

2 *FERMI*-LAT DATA: ANALYSIS AND RESULTS

2.1 Observations and data reduction

The *Fermi*-LAT is a pair-conversion telescope operating from 20 MeV to >300 GeV. It has a large peak effective area ($\sim$8000 cm^2 for 1 GeV photons), an energy resolution of typically $\sim$10 per cent and a field of view of about 2.4 sr with an angular resolution (68 per cent containment radius) better than 1° for energies above 1 GeV. Further details about the *Fermi*-LAT are given in Atwood et al. (2009).

The LAT data reported in this paper were collected from 2011 May 1 (MJD 556 82) to September 30 (MJD 558 34). During this time, the *Fermi* spacecraft operated almost entirely in survey mode. The analysis was performed with the ScienceTools software package version v9r27p1. The LAT data were extracted within a region of 20° radius centred at the location of PMN J0948+0022. Only events belonging to the 'source' class were used. The time intervals when the rocking angle of the LAT was greater than 52° were rejected. In addition, a cut on the zenith angle (<100°) was applied to reduce contamination from the Earth limb γ-rays, which are produced by cosmic rays interacting with the upper atmosphere. The spectral analysis was performed with the instrument response functions `P7SOURCE_V6` using an unbinned maximum-likelihood method implemented in the Science tool gtlike. A Galactic diffuse emission model and isotropic component, which is the sum of an extragalactic and residual cosmic ray background, were used to model the background.[1] The normalizations of both components in the background model were allowed to vary freely during the spectral fitting.

We analysed a region of interest of 10° radius centred at the location of PMN J0948+0022. We evaluated the significance of the γ-ray signal from the sources by means of a maximum-likelihood test statistic TS = 2 (logL_1–logL_0), where L is the likelihood of the data given the model with (L_1) or without (L_0) a point source at the position of PMN J0948+0022 (Mattox et al. 1996). Following the second *Fermi*-LAT source catalogue (2FGL; Nolan et al. 2012), the spectral model used for PMN J0948+0022 is a log parabola, $\mathrm{d}N/\mathrm{d}E \propto (E/E_0)^{-\alpha-\beta\,\log(E/E_0)}$ (Landau et al. 1986; Massaro et al. 2004), where the parameter α is the spectral slope at the energy E_0 and the parameter β measures the curvature around the peak. We fixed the reference energy E_0 to 272 MeV as in the 2FGL catalogue. The source model used in gtlike includes all of the point sources from the 2FGL catalogue that fall within 15° of PMN J0948+0022. The spectra of these sources were parametrized by power-law functions, $\mathrm{d}N/\mathrm{d}E \propto (E/E_0)^{-\Gamma}$, except for 2FGL J0909.1+0121, for which we used a log parabola as in the 2FGL catalogue. A first maximum-likelihood analysis was performed to remove from the model the sources having TS < 25 and/or a predicted number of counts based on the fitted model $N_\mathrm{pred} < 3$. A second maximum-likelihood analysis was performed on the updated source model. The fitting procedure has been performed with the sources within 10° of PMN J0948+0022 included with the normalization factors and the photon indices left as free parameters. For the sources located between 10° and 15° from our target, we kept the normalizations and the photon indices fixed to the values of the 2FGL catalogue.

2.2 Results

Integrating over the period 2011 May 1–September 30 (MJD 556 82–558 34), the fit yielded a TS = 674 in the 0.1–100 GeV

[1] http://fermi.gsfc.nasa.gov/ssc/data/access/lat/BackgroundModels.html

energy range, with an average integral flux of $(21.6 \pm 1.5) \times 10^{-8}$ ph cm^{-2} s^{-1}, a spectral slope $\alpha = 2.41 \pm 0.10$ and a curvature parameter around the peak $\beta = 0.20 \pm 0.06$. The corresponding apparent isotropic γ-ray luminosity is $\sim 1.8 \times 10^{47}$ erg s^{-1}. As a comparison during the first two years of *Fermi* operation (2008 August 4–2010 August 4), the average integral flux was $(9.2 \pm 0.5) \times 10^{-8}$ ph cm^{-2} s^{-1}, with a spectral slope $\alpha = 2.26 \pm 0.08$ and a curvature parameter around the peak $\beta = 0.26 \pm 0.06$ (Nolan et al. 2012). Thus, the average 0.1–100 GeV flux over 2011 May–September is about a factor of 2 higher than the 2FGL flux, but no significant spectral changes were observed.

Fig. 1 shows the γ-ray light curve for the period considered, using a log-parabola spectral model and 7 d time bins. For each time bin, the spectral parameters of PMN J0948+0022 and all sources within 10° of it were frozen to have the parameter values resulting from the likelihood analysis over the entire period. For the highest significance periods, we also reported as open circles the fluxes in 1 d time intervals. If TS < 10, 2σ upper limits were calculated. All uncertainties in measured γ-ray flux and index reported throughout this paper are statistical only. The systematic uncertainty in the effective area is energy dependent: it amounts to 10 per cent at 100 MeV, decreasing to 5 per cent at 560 MeV and increasing to 10 per cent above 10 GeV (Ackermann et al. 2012).

A daily peak flux of $(101 \pm 20) \times 10^{-8}$ ph cm^{-2} s^{-1} in the 0.1–100 GeV energy range was detected on 2011 June 20 (MJD 557 32), representing an increase of a factor of 5 with respect to the 2011 May–September average flux and more than an order of magnitude above the average 2FGL flux of the source. The corresponding apparent isotropic γ-ray luminosity is $\sim 8.8 \times 10^{47}$ erg s^{-1}. Preliminary results about this γ-ray flaring activity were reported by D'Ammando & Ciprini (2011) and Lucarelli et al. (2011). A second γ-ray flaring activity was observed at the end of 2011 July, peaking on July 28 (MJD 557 70) with a flux of $(87 \pm 25) \times 10^{-8}$ ph cm^{-2} s^{-1} in the 0.1–100 GeV energy range.

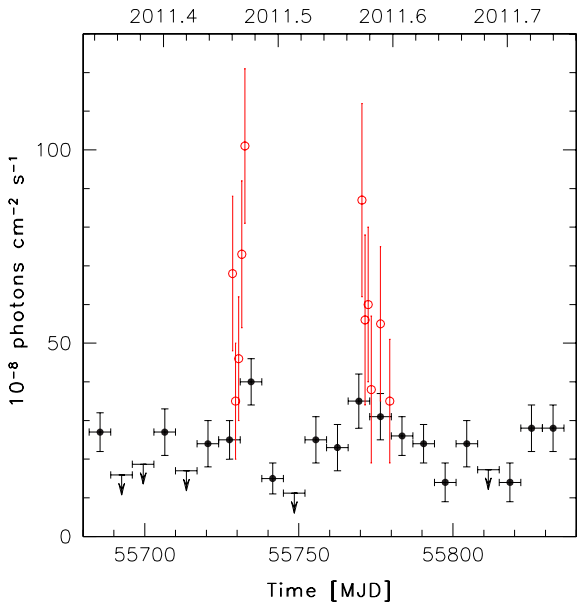

Figure 1. Integrated flux light curve of PMN J0948+0022 obtained by *Fermi*-LAT in the 0.1–100 GeV energy range during 2011 May 1–September 30 (MJD 556 82–558 34) with 7 d time bins. The arrows refer to 2σ upper limits on the source flux. Upper limits are computed when TS < 10. The open circles represent daily fluxes reported for the periods of high activity.

By means of the gtsrcprob tool, we estimated that the highest energy photon emitted from PMN J0948+0022 (with probability >80 per cent of being associated with the source) was observed on 2011 September 13 (MJD 558 17), at a distance of 0.°09 from the source and with an energy of 3.2 GeV. This suggests that this NLSy1 emits mainly at $E < 10$ GeV, even during flaring activity (see e.g. Foschini et al. 2011).

3 *SWIFT* DATA: ANALYSIS AND RESULTS

The *Swift* satellite (Gehrels et al. 2004) performed six observations of PMN J0948+0022 between 2011 April 29 and July 2. The observations were performed with all three on board instruments: the Burst Alert Telescope (BAT; Barthelmy et al. 2005, 15–150 keV), the X-ray Telescope (XRT; Burrows et al. 2005, 0.2–10.0 keV) and the Ultraviolet/Optical Telescope (UVOT; Roming et al. 2005, 170–600 nm). The hard X-ray flux of this source is below the sensitivity of the BAT instrument for the short exposures of these observations, and therefore, the data from this instrument were not used. Moreover, the source is not present in the *Swift*-BAT 70 month hard X-ray catalogue (Baumgartner et al. 2013).

3.1 *Swift*-XRT

The XRT data were processed with standard procedures (XRTPIPELINE v0.12.6), filtering and screening criteria by using the HEASOFT package (v6.12). The data were collected in photon counting mode for all of the observations. The source count rate was low (<0.5 counts s^{-1}); thus, pile-up correction was not required. Source events were extracted from a circular region with a radius of 20 pixel (1 pixel ∼ 2.36 arcsec), while background events were extracted from a circular region with radius of 50 pixel away from the source region or other bright sources. Ancillary response files were generated with `xrtmkarf` and account for different extraction regions, vignetting and point spread function corrections. We used the spectral redistribution matrices in the calibration data base maintained by HEASARC. When the number of photons collected was too low (<200 counts), the spectra were rebinned with a minimum of 1 count per bin and the Cash statistic (Cash 1979) was used. Since the effective area of *Swift*-XRT is a factor of ∼10 lower than that of the *XMM–Newton* European Photon Imaging Camera (EPIC), detailed spectral modelling was not performed with the XRT observations. The spectrum was fitted with an absorbed power law using the photoelectric absorption model TBABS (Wilms, Allen & McCray 2000), with a neutral hydrogen column density fixed to its Galactic value (5.07×10^{20} cm^{-2}; Kalberla et al. 2005). The fit results are reported in Table 1. The relatively harder X-ray spectrum observed for PMN J0948+0022 with respect to the other NLSy1s (e.g., Grupe et al. 2010; Zhou & Zhang 2010) could be due to the contribution of inverse Compton radiation from a relativistic jet, similarly to what is found in FSRQs. A photon index 1.4–1.5 was observed in X-rays also for another γ-ray NLSy1, SBS 0846+513 (D'Ammando et al. 2012a, 2013b).

3.2 *Swift*-UVOT

During the *Swift* pointings, the UVOT instrument observed PMN J0948+0022 in its optical (v, b and u) and UV ($w1$, $m2$ and $w2$) photometric bands. The data analysis was performed using the `uvotsource` task included in the HEASOFT package (v6.12).

Table 1. Log and fitting results of *Swift*-XRT observations of PMN J0948+0022 using an absorbed power-law model with an absorbing column density of $N_{\rm H} = 5.07 \times 10^{20}$ cm^{-2}.

Date (UT)	Date (MJD)	Net exposure time (s)	Photon index (Γ)	Flux 0.3–10 keV[a] ($\times 10^{-12}$ erg cm^{-2} s^{-1})
2011-04-29	556 80	1978	1.81 ± 0.19	4.3 ± 0.4
2011-05-15	556 96	4657	1.75 ± 0.15	4.5 ± 0.3
2011-05-28	557 09	3629	1.80 ± 0.16	4.8 ± 0.5
2011-06-04	557 16	2020	1.76 ± 0.20	3.5 ± 0.4
2011-06-14	557 26	5160	1.65 ± 0.16	3.7 ± 0.3
2011-07-02	557 44	2008	1.44 ± 0.17	5.9 ± 0.6

[a]Unabsorbed flux.

Table 2. Results of the *Swift*-UVOT observations of PMN J0948+0022.

Date (UT)	Date (MJD)	v	b	u	$w1$	$m2$	$w2$
2011-04-29	556 80	–	–	17.27 ± 0.03	–	–	–
2011-05-15	556 96	18.20 ± 0.13	18.43 ± 0.08	17.67 ± 0.07	17.46 ± 0.05	17.44 ± 0.06	17.46 ± 0.04
2011-05-28	557 09	18.05 ± 0.15	18.31 ± 0.09	17.48 ± 0.07	17.31 ± 0.05	17.35 ± 0.06	17.33 ± 0.04
2011-06-04	557 16	–	–	17.11 ± 0.03	–	–	–
2011-06-14	557 26	17.86 ± 0.11	18.31 ± 0.08	17.34 ± 0.06	17.34 ± 0.05	17.35 ± 0.05	17.29 ± 0.04
2011-07-02	557 44	–	–	17.64 ± 0.30	–	–	–

Source counts were extracted from a circular region of 5 arcsec radius centred on the source, while background counts were derived from a circular region of 10 arcsec radius in the source neighbourhood. We calculated the effective wavelengths, count rate to flux conversion factors and Galactic extinctions for the UVOT bands according to the procedure explained in Raiteri et al. (2010, 2011) and D'Ammando et al. (2012a). The observed magnitudes are reported in Table 2, and flux densities for the v, u and $w2$ filters are shown in Fig. 7. The optical u-band magnitude ranged from 17.67 to 17.11, with the peak detected on 2011 June 4 (MJD 557 16). No significant variability was observed in UV, but we noted that no UV observations were available during the optical peak in the u band.

4 *XMM–NEWTON* DATA: ANALYSIS AND RESULTS

4.1 Observations and data reduction

XMM–Newton (Jansen et al. 2001) observed PMN J0948+0022 on 2011 May 28–29 (MJD 557 09–557 10) for a total duration of 93 ks (observation ID 067370101, PI: D'Ammando). A simultaneous observation was performed by *Swift* on 2011 May 28.

The EPIC pn was operated in the large window mode, and the EPIC metal oxide semi-conductor (MOS) cameras (MOS1 and MOS2) were operated in the prime partial mode. The data were reduced using the *XMM–Newton* Science Analysis System (SAS v11.0.0), applying standard event selection and filtering. Inspection of the background light curves showed that strong flaring was present during the whole observation. The flaring time intervals were removed for the spectral analysis, leaving good exposure times of 36, 58 and 60 ks for the pn, MOS1 and MOS2, respectively. For each of the detectors the source spectrum was extracted from a circular region of radius 34 arcsec centred on the source and the background spectrum from a nearby region on the same chip. All the spectra were binned to contain at least 20 counts per bin to allow for χ^2 spectral fitting.

The Optical Monitor (OM) and Reflection Grating Spectrometers (RGS1 and RGS2) were also operating during the observation. No spectral lines were detected in the RGS spectra. This could be because the signal was rather low. The RGS data are not discussed further in this work. The data from the OM are discussed in Section 4.4.

4.2 X-ray spectral analysis

All spectral fits were performed over the 0.3–10 keV energy range using XSPEC v.12.7.1. The energies of spectral features are quoted for the rest frame of the source, while plots are in the observed frame, unless otherwise stated. All errors are quoted for 90 per cent confidence for one interesting parameter ($\Delta\chi^2 = 2.7$). The data from the three EPIC cameras were initially fitted separately, but since good agreement was found (<5 per cent), we proceeded to fit them together. As for the *Swift* spectra, Galactic absorption was included in all fits using the TBABS model. The results of all the fits are presented in Table 3. It is clear that a simple power-law model was insufficient to describe the data, while a broken power law yielded an acceptable fit (the improvement between the models is $\Delta\chi^2 = 969$ for two additional free parameters). The broken power law has a break at observed energy $E_{\rm break} = 1.72^{+0.09}_{-0.11}$ keV, with photon indices below and above the break of $\Gamma_1 = 2.14^{+0.03}_{-0.02}$ and $\Gamma_2 = 1.48^{+0.04}_{-0.03}$, respectively. In order to check for intrinsic absorption, a neutral absorber at the redshift of the source was added to this model, but it was found not to be required. The power-law slope above the break energy is significantly harder than those observed in radio-quiet NLSy1s (e.g., Grupe et al. 2010; Zhou & Zhang 2010), but similar to the slopes found in FSRQs (e.g., Donato et al. 2001). As already noted based on the *Swift*-XRT observations above, this makes highly probable that the emission from the jet dominates the X-ray spectrum at these energies. This conclusion is further supported by the fact that there was no detection of an Fe line in the spectrum. The 90 per cent upper limit on the equivalent width (EW) of a narrow emission line at 6.4 keV is EW<19 eV or 29 eV if the energy is allowed to vary between 6.4 and 7 keV.

On the other hand, the steeper slope found at low energies may be associated with the corona and the accretion disc of the system. In radio-quiet NLSy1s, the low-energy part of the spectrum is

Table 3. Summary of fits to the 0.3–10 keV *XMM–Newton* spectra. All fits also included absorption fixed at the Galactic value. Superscript *f* indicates that a parameter was kept fixed. See the text for a description of the models.

Model	Parameter	Value
Power law	Γ	1.88 ± 0.01
	Norm	$6.53 \pm 0.05 \times 10^{-4}$
	χ^2/d.o.f.	2342/1254
Broken power law	Γ_1	$2.14^{+0.03}_{-0.02}$
	$E_{\rm break}$ (keV)	$1.72^{+0.09}_{-0.11}$
	Γ_2	$1.48^{+0.04}_{-0.03}$
	Norm	$6.28 \pm 0.06 \times 10^{-4}$
	χ^2/d.o.f.	1373/1252
Power law +	Γ	1.44 ± 0.03
	PL norm	$4.13 \pm 0.17 \times 10^{-4}$
CompTT	T_0 (keV)	1.10×10^{-2f}
	$kT_{\rm e}$ (keV)	$0.50^{+0.16}_{-0.09}$
	τ	$10.2^{+0.3}_{-0.1}$
	Comp norm	$0.38^{+0.07}_{-0.06}$
	χ^2/d.o.f.	1329/1251
Power law (jet) +	$\Gamma_{\rm j}$	$1.21^{+0.07}_{-0.04}$
	PL norm$_{\rm j}$	$2.4^{+0.4}_{-0.2} \times 10^{-4}$
Power law (corona) +	$\Gamma_{\rm c}$	$2.53^{+0.14}_{-0.09}$
	PL norm$_{\rm c}$	$2.7^{+0.7}_{-0.4} \times 10^{-4}$
Blurred reflection	q	3^f
	$R_{\rm in}$ ($r_{\rm g}$)	6^f
	$R_{\rm out}$ ($r_{\rm g}$)	400^f
	incl (deg)	3^f
	Fe/solar	1^f
	ξ (erg cm s^{-1})	3000^f
	Ref norm	$2.3^{+1.2}_{-0.9} \times 10^{-9}$
	χ^2/d.o.f.	1333/1251
Power law (jet) +	$\Gamma_{\rm j}$	$1.20^{+0.08}_{-0.09}$
	PL norm$_{\rm j}$	$2.4 \pm 0.4 \times 10^{-4}$
Power law (corona)	$\Gamma_{\rm c}$	$2.63^{+0.11}_{-0.10}$
	PL norm$_{\rm c}$	$3.7 \pm 0.05 \times 10^{-4}$
	χ^2/d.o.f.	1339/1252

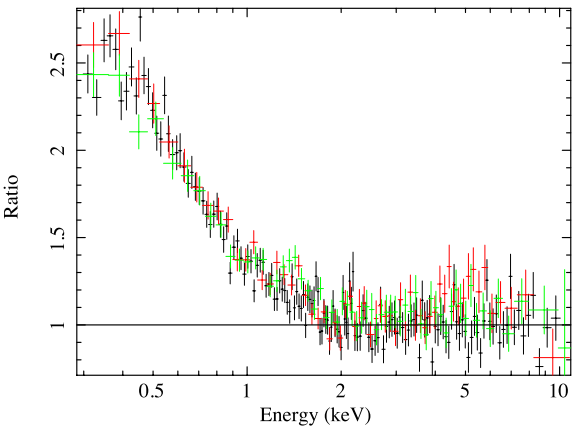

Figure 2. *XMM–Newton* EPIC pn (black), MOS1 (red) and MOS2 (green) data shown as a ratio to a power law with $\Gamma = 1.48$.

composed of a steep power law, originating in the corona, as well as a strong so-called soft excess, the origin of which is debated. Fig. 2 shows the spectrum of PMN J0948+0022 as a ratio to the power law with $\Gamma_2 = 1.48^{+0.04}_{-0.03}$, which fits the spectrum above the break energy, illustrating the strength of the soft component in this source.

The soft component can be fitted with a blackbody model with $kT \sim 0.18$ keV, which is within the typical range of temperatures for the soft excess (Gierlínski & Done 2004). However, it is well known that such a high temperature is inconsistent with standard accretion disc theory, which predicts that the thermal emission from the disc around a supermassive BH should peak in the ultraviolet band. Indeed, from the SED of the source (see e.g. Foschini et al. 2011, 2012), the observed emission from the accretion disc seems to peak at 20 eV, corresponding to a disc temperature of 11 eV in the rest frame of the source.

The soft X-ray emission may instead be due to Comptonization of the disc emission by a population of electrons with low temperature and large optical depth, which may exist in a transition region between the disc and the corona (Done et al. 2012). To investigate this model, we proceeded to fit the spectrum with a power law and a Comptonized blackbody, using the COMPTT model (Titarchuk 1994) and fixing the seed temperature at 11 eV. As seen in Table 3 and the left-hand panel of Fig. 3, this model provides a good fit to the spectrum, with best-fitting electron temperature $kT_{\rm e} = 0.50^{+0.16}_{-0.09}$ keV and optical depth $\tau = 10.2^{+0.3}_{-0.1}$. We note that allowing a higher seed temperature of 20 eV changes only the normalization of the Comptonized component, without significantly affecting any of the other best-fitting values presented in Table 3. The photon index of the power law in this model is $\Gamma_2 = 1.44 \pm 0.03$. In principle, the model should also contain a second power law to account for any emission from the corona, but such a component was not required in the fits.

An alternative explanation for the soft excess is that it is due to relativistically blurred reflection from the accretion disc. Such a model can explain the fact that the energy of the soft excess is observed to be fairly constant for BHs spanning several orders of magnitude in mass (Gierlínski & Done 2004; Bianchi et al. 2009), and has been successfully applied for a large number of sources (Crummy et al. 2006). In this picture, the X-ray spectrum of PMN J0948+0022 would be composed of a steep power law associated with the corona, a reflection component resulting from irradiation of the disc by this power law, as well as a hard power law associated with the jet, dominating at high energies. The large number of parameters in such a model are impossible to constrain with the available data, especially given that there is no Fe line or Compton hump for the reflection model to anchor to. To set some constraints on such a scenario, we constructed a model made of two power laws (with the photon indices constrained to be steeper and flatter than 2, for the corona and jet, respectively) together with a relativistically blurred reflection component with parameters fixed at 'standard' values. The reflection was modelled with KDBLUR acting on the REFLIONX model by Ross & Fabian (2005), with the photon index of the illuminating power law tied to the steep power law. The inner and outer radii of the disc were fixed at 6 gravitational radii ($r_{\rm g}$) and 400 $r_{\rm g}$, respectively. Solar abundances were assumed and the emissivity index was fixed at $q = 3$ (i.e. assuming a standard emissivity profile of r^{-3} from a central point source). The inclination was fixed at $i = 3^\circ$, which is the angle of the jet inferred by Foschini et al. (2011). The disc may not be exactly perpendicular to the jet, but we note that allowing a larger value, i.e. up to around $i = 15^\circ$, did not change the results. After optimization, the ionization state of the disc was fixed at $\xi = 3000$ erg cm s^{-1}. As seen in Table 3, this model results in a fit of quality comparable to the Comptonized blackbody. However, it should be noted that it is the steep power law and not the reflection component that provides

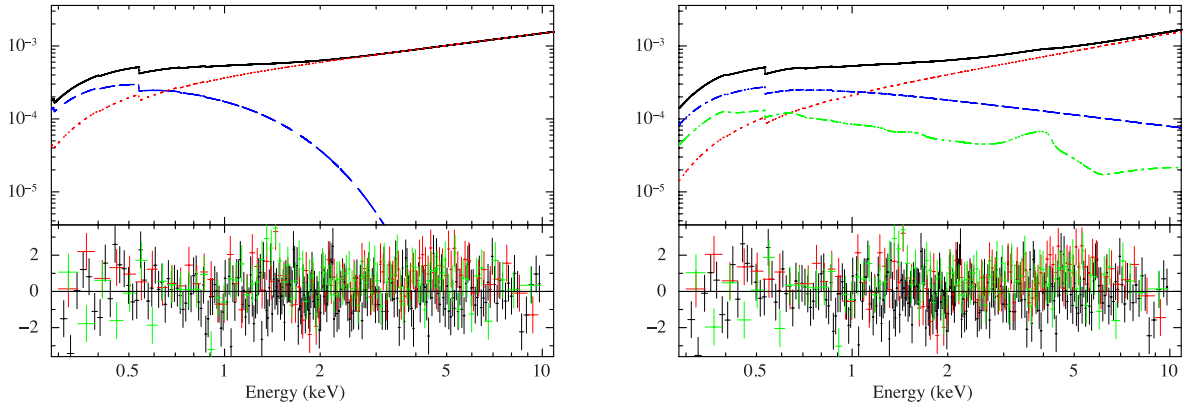

Figure 3. Components of the best-fitting models from Table 3 together with the residuals of the fits. Left: Comptonized blackbody (blue, dashed line), power law (red, dotted line) and their sum (black, solid line). Right: steep power law (blue, dashed line), its associated reflection spectrum (green, dash–dotted line), hard power law (red, dotted line) and their sum (black, solid line). In the lower panels, the black, red and green points represent data from pn, MOS1 and MOS 2, respectively.

most of the flux at low energies, as seen in Fig. 3, which shows the model components. In fact, a fit with two power laws but no reflection is only marginally worse ($\Delta\chi^2 = 6$ for one more degree of freedom, see Table 3). Allowing each of the parameters of the reflection model to vary did not significantly change these results.

4.3 X-ray variability

The EPIC pn light curve is shown in Fig. 4, with the time intervals with low background that were used for the spectral analysis marked in red. The source was only mildly variable during the *XMM* observation, as suggested by the count rate light curve. The observed fluxes corrected for Galactic absorption are $F_{2-10\mathrm{keV}} = (2.56 \pm 0.05) \times 10^{-12}$ erg cm^{-2} s^{-1} and $F_{0.3-10\mathrm{keV}} = 4.59^{+0.03}_{-0.05} \times 10^{-12}$ erg cm^{-2} s^{-1}, in agreement with the *Swift*-XRT results (see Table 1).

The root-mean-square (rms) variability spectrum of the observation is shown in Fig. 5, and it is calculated following Vaughan et al. (2003) using light curves with 0.5 ks bins. The rms spectrum shows the variability amplitude of the source as a function of energy, corrected for the variance due to measurement errors and normalized by the mean count rate in each energy band. The error bars represent the uncertainty expected from the Poisson noise (Vaughan et al. 2003). Since the flaring background becomes increasingly dominant with energy, we plot the rms spectrum only up to 5 keV (at which energy, the ratio of signal to background is about 4). The variability clearly decreases with energy up to around 1.7 keV, but then starts to increase again. It is interesting to note that this break coincides with the break energy of the broken power-law model (see Table 3), since it is consistent with our interpretation that the Seyfert and jet components dominate at low and high energies, respectively (see further Section 7.3). The rms spectrum presented in Bhattacharyya et al. (2013) has a different energy binning, but exhibits an overall shape that is consistent with our results. While we find that the increase in rms variability above ∼2 keV is not affected by our choice of energy binning, it will be important to confirm these results with an observation where the variability analysis can be extended to higher energies.

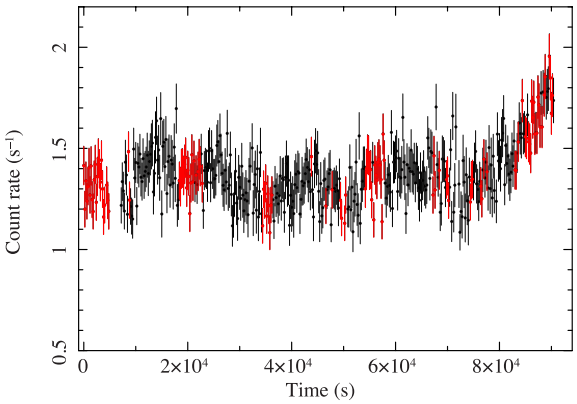

Figure 4. 0.2–10 keV EPIC pn light curve on a 200 s time-scale, using only fully exposed bins. The time periods used for the spectral analysis are marked in red. The remaining time intervals were severely affected by background flaring.

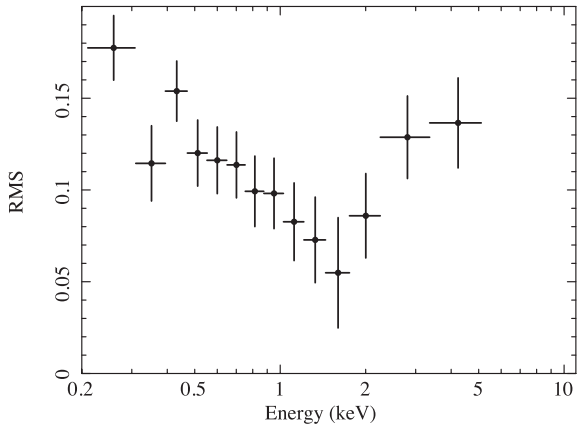

Figure 5. rms variability spectrum of the *XMM–Newton* observation of PMN J0948+0022, calculated using 0.5 ks bins.

We further investigated the spectral variability by fitting the broken power-law model to spectra extracted in 15 ks intervals (corresponding to 3–7.5 ks of good exposure time per spectrum). Fig. 6 shows the evolution of the best-fitting parameters and the flux as a function of time. There are no systematic trends with time and only the flux is found to vary significantly above the 3σ level. However, the photon index and E_{break} are found to be marginally variable (>90 per cent CL).

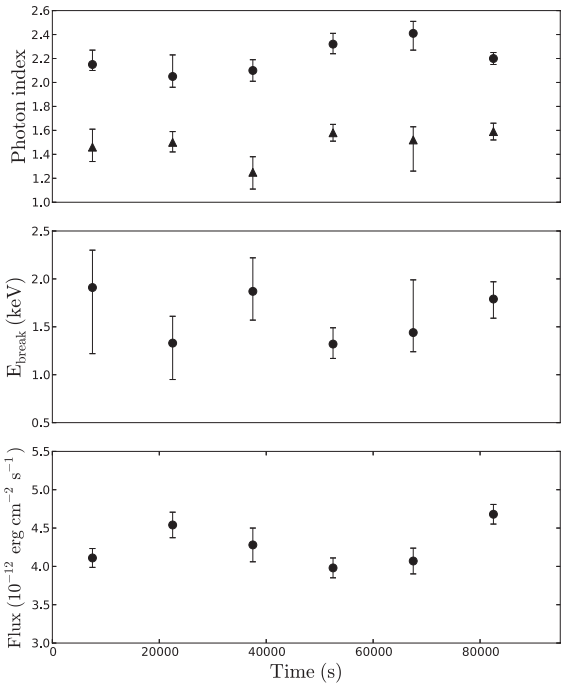

Figure 6. Results of fits to time-resolved spectra of the *XMM–Newton* observation using a broken power-law model. The top panel shows the temporal evolution of the photon indices (the indices below and above the break energy are shown as filled circles and filled triangles, respectively), the middle panel shows the break energy and the bottom panel shows the 0.3−10 keV unabsorbed flux derived from the fits.

4.4 Optical Monitor data

The OM (Mason et al. 2011) on board *XMM–Newton* is a 30 cm telescope carrying six optical/UV filters and two grisms. Observations of PMN J0948+0022 in 2011 May 28–29 consisted of 7 subsequent exposures in v band, followed by 10 in b band, 9 in u band, 10 in $w1$ band and $m2$ band, then 5 in $w2$ band. All optical exposures were 800 s long, while UV exposures were 1600 and 2700 s long. We used the SAS task `omichain` to reduce the data and the tasks `omsource` and `omphotom` to derive the source magnitude. Average observed magnitudes are $v = 18.28 \pm 0.06, b = 18.63 \pm 0.02, u = 17.64 \pm 0.02$, $w1 = 17.27 \pm 0.02, m2 = 17.24 \pm 0.03$ and $w2 = 17.22 \pm 0.11$. The difference of 0.2–0.3 mag in the optical filters with respect to the *Swift*-UVOT observations performed on 2011 May 28 at least partially could be due to the source variability.

5 GROUND-BASED OPTICAL AND INFRARED OBSERVATIONS

5.1 CRTS

The source has been monitored by the CRTS[2] (Drake et al. 2009; Djorgovski et al. 2011), using the 0.68 m Schmidt telescope at Catalina Station, AZ, and an unfiltered CCD. The typical cadence is four exposures separated by 10 min in a given night; this may be repeated up to four times per lunation, over a period of ∼6–7 months each year, while the field is observable. Photometry is obtained using the standard SOURCE-EXTRACTOR package (Bertin & Arnouts 1996) and transformed from the unfiltered instrumental magnitude to Cousins V by $V = V_{CSS} + 0.31(B - V)^2 + 0.04$ with a scatter of 0.056 mag.[3] The flux densities collected by CRTS in the V band are reported in Fig. 7.

Table 4. Results of the INAOE observations of PMN J0948+0022 in J, H and K bands.

Date (MJD)	J (mJy)	H (mJy)	Ks (mJy)
556 77.219	0.864 ± 0.026	1.248 ± 0.075	1.234 ± 0.136
556 89.243	–	0.721 ± 0.065	–
556 93.171	–	0.400 ± 0.020	–
556 94.139	0.469 ± 0.028	0.601 ± 0.024	0.929 ± 0.084
556 96.181	–	0.380 ± 0.030	
557 02.163	0.316 ± 0.016	0.331 ± 0.020	0.762 ± 0.084
557 03.139	0.866 ± 0.069	1.530 ± 0.138	

5.2 INAOE

NIR observations of PMN J0948+0022 were performed during 2011 April–May, at the 2.1 m telescope 'Guillermo Haro', with the NIR Cananea Near Infrared Camera, (CANICA) equipped with a Rockwell 1024 × 1024 pixel Hawaii infrared array, working at 75.4 K, with standard J(1.164–1.328 μm), H(1.485–1.781 μm) and Ks (1.944–2.294 μm) filters. The plate scale is 0.32 arcsec pixel^{-1}. Observations were carried out in series of 10 dithered frames in each filter. Data sets were coadded after correcting for bias and flat-fielding. Flats were obtained from sky frames derived from the dithered ones. Magnitudes in J, H and Ks filters are reported in Table 4. The flux densities collected in the J and H bands are reported also in Fig. 7.

6 RADIO OBSERVATIONS

6.1 Effelsberg 100 m

The radio spectrum of PMN J0948+0022 was observed with the Effelsberg 100 m telescope between 2011 May 24 and October 1 within the framework of a *Fermi*-related monitoring programme of γ-ray blazars [*Fermi*-GST AGN multi-frequency monitoring alliance (F-GAMMA) programme; Fuhrmann et al. 2007]. The measurements were conducted with the secondary focus heterodyne receivers at 2.64, 4.85, 8.35, 10.45, 14.60, 23.05 and 32.00 GHz. The observations were performed quasi-simultaneously with cross-scans, that is, slewing over the source position, in azimuth and elevation directions, with adaptive numbers of subscans for reaching the desired sensitivity (for details see Angelakis et al. 2008; Fuhrmann et al. 2008). Corrections for pointing offset, gain, atmospheric opacity and sensitivity have been applied to the data. The different spectra collected by Effelsberg are represented in Fig. 8.

Radio spectra and fluxes indicate that the source was highly active already in 2011 May 24 (MJD 557 05), before the first peak of the γ-ray activity, followed by a flux decrease and a flattening of the spectrum in 2011 August–October. The spectral index calculated between 8.4 and 32 GHz changes between -0.4 ± 0.1 and 0.2 ± 0.1 from 2011 May to October. No significant flux changes were observed at frequencies below 8.4 GHz. This is likely due to opacity effects at the low frequencies. Flux densities at 32 and 14.6 GHz are also shown in Fig. 7.

[2] http://crts.caltech.edu

[3] http://nesssi.cacr.caltech.edu/DataRelease/FAQ2.html#improve

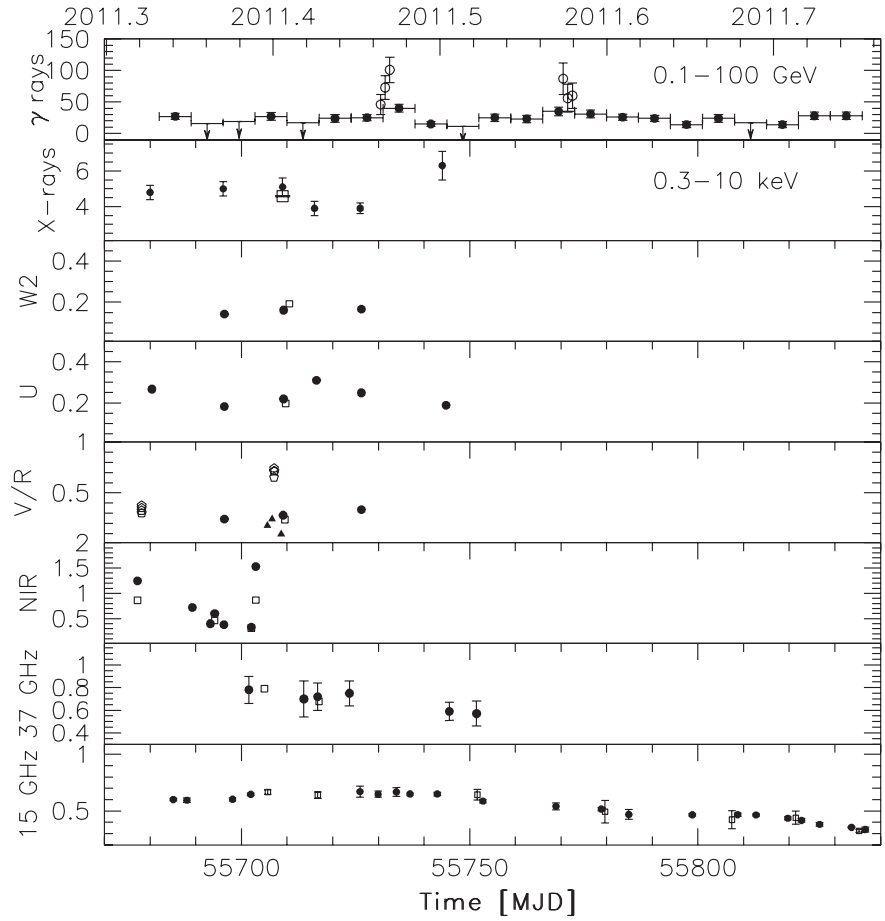

Figure 7. Multifrequency light curve of PMN J0948+0022 for the period 2011 May 1–September 30 (MJD 556 82–558 34) collected (from top to bottom) in: γ-rays by *Fermi*-LAT (0.1–100 GeV; in units of 10^{-8} ph cm^{-2} s^{-1}); X-rays by *Swift*-XRT (filled circles) and *XMM–Newton* (open square) (0.3–10 keV; in units of 10^{-12} erg cm^{-2} s^{-1}); $w2$ band by *Swift*-UVOT (filled circles) and *XMM*-OM (open square); u band by *Swift*-UVOT (filled circles) and *XMM*-OM (open square); V band by *Swift*-UVOT (filled circles), *XMM*-OM (open square) and CRTS (open pentagons) and R band taken from Eggen, Miller & Maune (2013; filled triangles); J (open squares) and H (filled circles) bands by INAOE; 37 GHz by Metsähovi (filled circles) and 32 GHz by Effelsberg (open squares); 15 GHz by OVRO (filled circles) and Effelsberg (open squares). The flux densities collected from $w2$ to NIR are reported in units of mJy, from 37 GHz to 15 in units of Jy. In the top panel, daily integrated γ-ray fluxes are reported as open circles.

6.2 Metsähovi

Observations at 37 GHz were made with the 13.7 m Metsähovi radio telescope, which is a radome enclosed paraboloid antenna situated in Finland. The measurements were made with a 1 GHz-band dual beam receiver centred at 36.8 GHz. The observations are ON–ON measurements, alternating between the source and the sky in each feed horn. A typical integration time to obtain one flux density data point is between 1200 and 1400 s. The detection limit at 37 GHz is of the order of 0.2 Jy under optimal conditions. Data points with a signal-to-noise ratio <4 are handled as non-detections. The flux density scale is set by observations of DR 21. Sources NGC 7027, 3C 274 and 3C 84 are used as secondary calibrators. A detailed description of the data reduction and analysis is given in Teräsranta et al. (1998). The error on the flux density includes the contribution from the measurement rms and the uncertainty of the absolute calibration. Flux densities at 37 GHz are shown in Fig. 7.

6.3 OVRO 40 m

As part of an ongoing blazar monitoring programme, the OVRO 40 m radio telescope has observed PMN J0948+0022 at 15 GHz regularly since the end of 2007 (Richards et al. 2011). This monitoring programme includes about 1700 known and likely γ-ray loud blazars above declination -20°. The sources in this programme are observed in total intensity twice per week with a 4 mJy (minimum) and 3 per cent (typical) uncertainty on the flux densities. Observations were performed with a dual-beam (each 2.5 arcmin FWHM) Dicke-switched system using cold sky in the off-source beam as the reference. Additionally, the source is switched between beams to reduce atmospheric variations. The absolute flux density scale is calibrated using observations of 3C 286, adopting the flux density (3.44 Jy) from Baars et al. (1977). This results in about a 5 per cent absolute scale uncertainty, which is not reflected in the plotted errors. During the OVRO monitoring, the flux density varied from 671 mJy (on MJD 557 25; 2011 June 13) to 335 mJy (on MJD 558 36; 2011 October 2), as shown in Fig. 7.

6.4 Medicina

PMN J0948+0022 was observed with the 32 m Medicina radio telescope eight times between 2011 May and October. The new enhanced single-dish control acquisition system, which provides

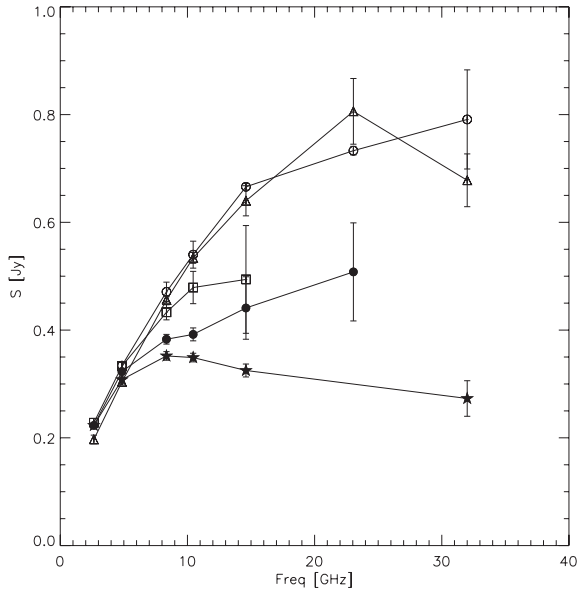

Figure 8. Radio spectra of PMN J0948+0022 collected from 2.64 and 32 GHz by Effelsberg in 5 epochs: 2011 May 24 (MJD 557 05; empty circles), 2011 June 5 (MJD 557 17; empty triangles), 2011 August 6 (MJD 557 79; empty squares), 2011 September 17 (MJD 558 21; filled circles) and 2011 October 1 (MJD 558 35; filled stars).

Table 5. Results of the Medicina radio observations at 5 and 8.4 GHz of PMN J0948+0022.

Date (UT)	Date (MJD)	$S_{5\,\mathrm{GHz}}$ (Jy)	$S_{8.4\,\mathrm{GHz}}$ (Jy)
2011-06-12	557 24	0.37 ± 0.02	0.38 ± 0.02
2011-07-29	557 71	–	0.35 ± 0.02
2011-08-01	557 74	0.35 ± 0.02	0.45 ± 0.02
2011-08-10	557 83	0.45 ± 0.05	0.39 ± 0.05
2011-09-08	558 12	0.35 ± 0.02	–
2011-09-22	558 26	0.34 ± 0.02	–
2011-10-13	558 47	0.33 ± 0.05	–
2011-11-16	558 81	0.25 ± 0.05	–

enhanced sensitivity and supports observations with the cross-scan technique, was used. Observations were performed at both 5 and 8.4 GHz; the typical on-source time was 1.5 min and the flux density was calibrated with respect to 3C 286. Since the signal-to-noise ratio in each scan across the source was low (typically ∼3), we performed a stacking analysis of the scans, which allowed us to significantly improve the signal-to-noise ratio and the precision of the measurement. The flux densities at 5 and 8.4 GHz are reported in Table 5. The peak of the flux density was observed by Medicina, first at 8.4 GHz on 2011 August 1 (MJD 557 74) and then at 5 GHz on August 10 (MJD 557 83), about 7–8 weeks after the peak observed at 15 GHz by OVRO. Using the Medicina data at 5 and 8.4 GHz together with the nearest OVRO observation spectral indices of -0.54 ± 0.04, -0.36 ± 0.03 and -0.04 ± 0.06 were measured for 2011 June 12, August 1 and 10, respectively, suggesting a radio spectral evolution in agreement with the behaviour observed by Effelsberg.

6.5 MOJAVE: data analysis and results

We investigated the parsec-scale morphology and flux density variability at 15 GHz by means of 5 epoch VLBA data from the MOJAVE programme (Lister et al. 2009). The data sets span the time interval between 2011 February and December, in order to overlap with the *Fermi*-LAT data. We imported the calibrated *uv* data into the National Radio Astronomy Observatory AIPS package. In addition to the total intensity images, we produced the Stokes *Q* and *U* images, to derive information on the polarized emission. The flux density was derived by means of the AIPS task JMFIT which performs a Gaussian fit on the image plane. Total intensity flux density and polarization information are reported in Table 6. During some observing epochs, we detected a hint of the jet emerging from the core component with a position angle of ∼30° (see Figs 9 and 10),

Table 6. Flux density and polarization of PMN J0948+0022 from 15 GHz MOJAVE data.

Date (UT)	Date (MJD)	S_{Core} (mJy)	S_{Jet} (mJy)	S_{pol} (mJy)	S_{pol} (per cent)	EVPA (deg)
2011-02-20	556 12	622	3	5	0.8	25
2011-05-26	557 07	659	6	13	2.0	51
2011-06-24	557 36	665	6	14	2.1	49
2011-09-12	558 16	458	–	6	1.3	44
2011-12-12	559 07	380	–	2	0.5	67

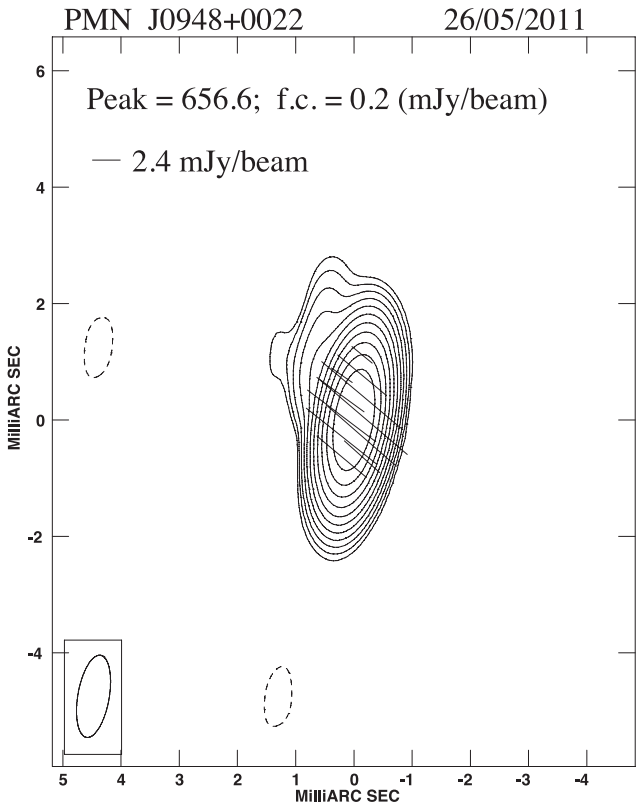

Figure 9. VLBA image at 15.3 GHz of PMN J0948+0022 collected on 2011 May 26. In the image, we provide the restoring beam, plotted in the bottom-left corner, the peak flux density in mJy/beam and the first contour (f.c.) intensity in mJy/beam, which is three times the off-source noise level. Contour levels increase by a factor of 2. The vectors superimposed on the total intensity contours show the percentage polarization and the position angle of the electric vector.

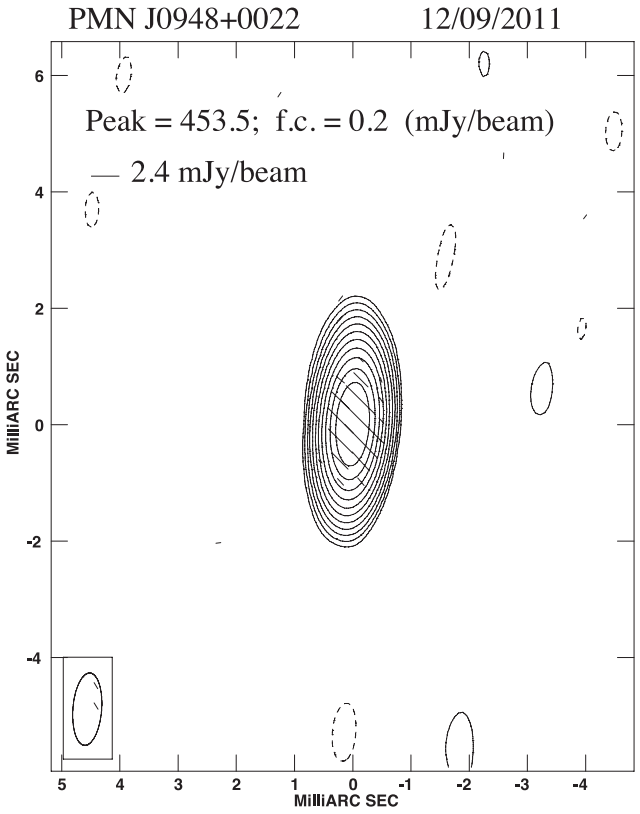

Figure 10. VLBA image at 15.3 GHz of PMN J0948+0022 collected on 2011 September 12. In the image, we provide the restoring beam, plotted in the bottom-left corner, the peak flux density in mJy/beam and the first contour (f.c.) intensity in mJy/beam, which is three times the off-source noise level. Contour levels increase by a factor of 2. The vectors superimposed on the total intensity contours show the percentage polarization and the position angle of the electric vector.

in agreement with previous works (e.g., Doi et al. 2006; Giroletti et al. 2011). In accordance with the flux density observed by OVRO at 15 GHz, a clear decrease of the flux density was observed by MOJAVE from 657 mJy on 2011 May 26 (MJD 557 07) to 378 mJy on 2011 December 12 (MJD 559 07). In addition, a higher polarized emission ($S_{\rm pol}$) and polarization percentage was observed on May 26 with respect to December 12 (Table 6). On the other hand, the electric vector position angle (EVPA) of the core does not change significantly, ranging between 25° and 67°.

7 DISCUSSION AND CONCLUSIONS

PMN J0948+0022 is the best studied γ-ray NLSy1 (see e.g. Abdo et al. 2009c; Foschini et al. 2012). Simultaneous multiwavelength observations presented here allow a broad-band characterization of this source, including the first *XMM–Newton* observation of this NLSy1.

7.1 Behaviour of the light curves

In Fig. 7, we compare the γ-ray light curve collected by *Fermi*-LAT in the 0.1–100 GeV energy range to the X-ray (0.3–10 keV), UV ($w2$ filter), optical (V, R and u filters), NIR (J and H filters) and radio (37 and 15 GHz) light curves collected by *Swift*, *XMM*, CRTS, Instituto Nacional de Astrofisica, Optica y Electronica (INAOE), Metsähovi, Effelsberg and OVRO. Strong variability was observed in γ-rays, with two flaring periods peaked on 2011 June 20 and July 28 and a variability amplitude (calculated as the ratio of maximum to minimum flux) of ∼10. Such a variability amplitude as well as the rapid flaring episodes and high apparent isotropic γ-ray luminosity (∼10^{48} erg s^{-1} at the peak) observed in 2011 are typical of FSRQs. During the *Swift* observations, PMN J0948+0022 was observed in an intermediate X-ray state (0.3–10 keV flux of 3.5–5.9 × 10^{-12} erg cm^{-2} s^{-1}) between the highest flux observed from this source on 2012 December 30 during a γ-ray flaring activity (12.6 × 10^{-12} erg cm^{-2} s^{-1}; see D'Ammando & Orienti 2013) and the low flux observed on 2008 December 8 (2.2 × 10^{-12} erg cm^{-2} s^{-1}; Abdo et al. 2009a). A clear increase of the flux was observed between 2011 June 14 (MJD 557 26) and July 2 (MJD 557 44), after the γ-ray flare observed by LAT. The flux increase was accompanied by a hardening of the X-ray spectrum. However, the lack of X-ray data during the peaks of the γ-ray activity does not allow us to draw conclusions regarding a contemporaneous increase of the activity in X-ray and γ-rays.

The source increased its V-band flux by a factor of ∼3 from 2011 May 15 (MJD 556 96) to May 26 (MJD 557 07). An increase of flux density between 2011 May 24 and 25 of about 50 per cent in R band was reported by Eggen et al. (2013), with a significant decrease of a factor of ∼3.5 in two days. These rapid changes are in agreement with the optical intraday variability observed in 2011 March 27–31, with a total amplitude of ∼0.9 mag during ∼4 h on April 1 (Maune, Miller & Eggen 2013). Similar intraday variability has been reported for this source by Liu et al. (2010); Maune, Miller & Eggen (2011); Paliya et al. (2013) and Itoh et al. (2013), indicating a relativistic jet as the most likely origin for the optical emission in PMN J0948+0022. If this variability is due to the accretion disc, the amplitude variability should be higher during faint states, when the jet activity is lower, and minimized during bright states, as already discussed in Maune et al. (2011). At the time of the optical peak on 2011 May 25, a high optical polarization percentage (P = 12.31 per cent) was observed, with a significant increase with respect to the observation performed in May 24 (P = 1.35 per cent) (Eggen et al. 2013). An increase of polarization percentage from 0.8 per cent on 2011 February 20 to 2.0 per cent on May 26 was also observed in the MOJAVE data (see Section 6.5).

The sparse sampling of the optical and NIR light curves does not allow us to make a detailed comparison with the γ-ray and radio light curves. However, it is worth noting that an increase of flux density was also observed in NIR in 2011 mid-May (about MJD 557 00), with no counterpart in γ-rays. In fact, PMN J0948+0022 was quite active in the H band on 2011 April 26 (MJD 556 77), and after a decrease in the following 3 weeks, we observed on 2011 May 22 (MJD 557 03) a significant increase by a factor of ∼4.5 in 24 h. A similar behaviour seems to be observed in the J band, with an increase by a factor of ∼2.5 on May 22 (MJD 557 03). On the other hand, no significant variability was observed in UV during the *Swift*-UVOT observations, probably due to the accretion disc emission that dilutes the variability in that part of the spectrum.

During the OVRO monitoring, the flux density at 15 GHz changed more smoothly than at higher energies, with an amplitude variability of ∼2 between 670 mJy (2011 June 13; MJD 557 25) and 335 mJy (2011 October 2; MJD 558 36) and a gradual decrease. A flaring activity seems to start before the first γ-ray flare, with a peak at about MJD 557 00, close to the optical and NIR flare, and a monotonic decreasing trend in the following months at 15 and 37 GHz. In the same way, the radio spectra collected by Effelsberg, Medicina and OVRO showed a significant spectral evolution with

a high-frequency component dominating the emission in 2011 May. A similar spectral evolution was already reported in Angelakis et al. (2013) for PMN J0948+0022 and other γ-ray-emitting NLSy1s with variability patterns typical of relativistic jets and thus similar to blazars.

The different behaviour observed in the radio-to-optical and the γ-ray energy bands could be related to a bending and inhomogeneous jet, as proposed for some blazars (e.g., Raiteri et al. 2010, 2011), with a variable misalignment between the zone responsible for the radio-to-optical emission and the zone responsible for γ-rays. The change of the viewing angle of the different emitting regions may produce a change of the Doppler factor, with the Doppler boosting of the radio-to-optical emission increasing first, followed by an increase of the Doppler boosting of the γ-ray emission. This complex behaviour also could be in agreement with the turbulent extreme multicells scenario proposed by Marscher (2012). Alternatively, the radio activity could be related to the γ-ray flaring activity observed in 2010 July–August, but the large delay of about 1 yr makes this hypothesis unlikely. The sparse and irregular sampling, especially from NIR to X-rays, does not allow us to test the different scenarios.

7.2 Energetics

The high apparent isotropic γ-ray luminosity observed for PMN J0948+0022 in 2011 May–September ($\sim 1.8 \times 10^{47}$ erg s^{-1}) should reflect a small viewing angle with respect to the jet axis and thus high beaming factors, similarly to what is observed for the FSRQs and also for the NLSy1 SBS 0846+0513 (D'Ammando et al. 2012a, 2013b). This is consistent with the viewing angle of 3° used for modelling the SEDs of this source in Foschini et al. (2011, 2012). In contrast, most of the radio galaxies detected by the LAT have an apparent isotropic γ-ray luminosity lower than 10^{46} erg s^{-1}, suggesting a smaller beaming factor and possibly a different structure of the jet (Abdo et al. 2010). Assuming a BH mass of 10^8 M$_\odot$ (but see Section 7.5), we obtain an Eddington luminosity of 1.3×10^{46} erg s^{-1}. During the 2011 June flare, PMN J0948+0022 reached an apparent isotropic γ-ray luminosity of $L_\gamma = 8.8 \times 10^{47}$ erg s^{-1}, making the radiative power $L_{\rm rad} = L_\gamma/\Gamma^2 = 3.5 \times 10^{45}$ erg s^{-1}, assuming a quite typical value for this source of $\Gamma = 16$ (Foschini et al. 2011, 2012). This is about 25 per cent of the Eddington luminosity, comparable to the values observed for bright FSRQs detected by LAT (see e.g. Nemmen et al. 2012).

7.3 X-ray spectrum

Thanks to the first high-quality *XMM–Newton* observation of PMN J0948+0022, we are able to study in detail its X-ray spectrum (see Section 4.2). The spectral modelling of the *XMM* data of PMN J0948+0022 showed that emission from the jet most likely dominates the spectrum above ∼2 keV, while the emission from the underlying Seyfert galaxy can be seen at lower energies. Interestingly, the observation of such a component, typical in the X-ray spectra of radio-quiet NLSy1s, is quite unusual in jet-dominated AGNs, even if not unique (e.g., the FSRQ PKS 1510−089; Kataoka et al. 2008). Contrary to what is observed in some blazars (e.g., BL Lacertae; Raiteri et al. 2010), no excess absorption above the Galactic column density was necessary by the fit for modelling the low-energy part of the spectrum (Grupe et al. 2010). As well as for PKS 1510−089, we hypothesize that the emission below 2 keV was mainly due to the soft X-ray excess. However, we cannot distinguish between different models for the soft X-ray emission on a statistical basis. Models where the soft emission is partly produced by blurred reflection, or Comptonization of the thermal disc emission, or simply a steep power law, all provide good fits to the data. Our reflection model differs substantially from that presented by Bhattacharyya et al. (2013). While we confirm that their model is a good fit to the spectrum, we note that it relies on a high inclination angle of $i = 74°$, which is inconsistent with the blazar like properties of the source, as well as the inclusion of a warm absorber, which is not required in any of the other models. Furthermore, their model does not allow the power law, which illuminates the disc, to also contribute directly to the spectrum.

A blackbody model also gives a comparable fit, but a temperature of $kT = 0.18$ keV is necessary. Such a high temperature is inconsistent with the standard accretion disc theory (see e.g. Shakura & Sunyaev 1973). Further long-duration X-ray observations with *XMM–Newton*, *Suzaku* and *NuSTAR*, preferably when the source is in a low γ-ray state, will be needed to place stronger constraints on these models.

Our interpretation that the X-ray emission above 2 keV is produced by the jet is also supported by the rms spectrum (Fig. 5), which shows a break at 1.7 keV, above which the variability increases with energy. While Seyfert galaxies typically exhibit rms spectra decreasing with energy above ∼1–2 keV (Markowitz et al. 2004; Ponti et al. 2007; Chitnis et al. 2009), the opposite behaviour is often observed in blazars (e.g., Ravasio et al. 2004; Gliozzi et al. 2006). It should be noted, however, that there is no one-to-one correlation between the rms spectrum and AGN type and that rms spectra often change substantially with time (as seen in e.g. Gliozzi et al. 2006; Larsson et al. 2008).

The spectrum of PMN J0948+0022 changed from a steep slope of $\Gamma \sim 2.1$ to a much harder one of $\Gamma \sim 1.5$ above 1.7 keV. A similar spectrum has also been observed in the *XMM* observation of the γ-ray NLSy1 PKS 2004–447 (Gallo et al. 2006). An X-ray spectrum unusually hard for an NLSy1 was observed by *Swift*-XRT in SBS 0846+513 (D'Ammando et al. 2012a, 2013b) and PKS 1502+036 (D'Ammando et al. 2013a), two other NLSy1s detected by LAT. Models more complex than the simple power law were not applicable in these cases due to insufficient statistics, in particular below 1–2 keV. Thus, the 0.3–10 keV spectra collected by *Swift*-XRT seem to be dominated by the jet emission.

The small variability amplitude (∼2) observed in X-rays with respect to the γ-rays (∼10) could be an indication that the X-ray emission is produced by the low-energy tail of the same electron distribution. On the other hand, the peak flux in X-rays was observed on 2011 July 2 during a period of low γ-ray activity, suggesting that different mechanisms could be at work in the X-ray and γ-ray bands (e.g., synchrotron self-Compton and external Compton, respectively). The presence of the soft X-ray excess below 2 keV could dilute the X-ray variability over the 0.3–10 keV energy range, but an amplitude variability of a factor of ∼2 (with fluxes between 2.1–4.1×10^{-12} erg cm^{-2} s^{-1}) was also observed considering only the 2–10 keV energy range. In this context, no obvious relation exists between the soft X-ray excess and the γ-ray emission. An intriguing possibility is that the excess observed below 2 keV is a signature of the bulk Comptonization process by a cold relativistic plasma accelerating along the jet and scattering on disc photons reprocessed by the broad-line region (BLR; Celotti, Ghisellini & Fabian 2007). A dedicated modelling of the source's SED including *XMM–Newton* and *Fermi*-LAT data will be presented in a forthcoming paper.

7.4 Host galaxy

The discovery of a relativistic jet in a class of AGN thought to be hosted in spiral galaxies such as the NLSy1s, as opposed to blazars and radio galaxies hosted in elliptical galaxies (Blandford & Rees 1978), was a great surprise challenging the current knowledge on how the jet structures are generated and developed (see e.g. Böttcher & Dermer 2002; Marscher 2010). Unfortunately only very sparse observations of the host galaxies of radio-loud NLSy1s are available and the sample of objects studied by Deo, Crenshow & Kraemer (2006) and Zhou et al. (2006) have redshifts $z < 0.03$ and 0.1, respectively, while four out five of the NLSy1s detected in γ-rays have $z > 0.2$. Among the radio-loud NLSy1s detected up to now by LAT, only for the closest one, 1H 0323+342, was the host galaxy clearly detected. Observations with the *Hubble Space Telescope* and Nordic Optical Telescope revealed a one-armed galaxy morphology or a circumnuclear ring, respectively, suggesting two possibilities: the spiral arm of the host galaxy Zhou et al. (2007) or the residual of a galaxy merger (Anton, Browne & Marcha 2008). These observations, together with the lack of information about the host galaxy of the other γ-ray-emitting NLSy1s, leaves room for the hypothesis that the NLSy1s detected in γ-rays by LAT could have peculiar host galaxies with respect to the other NLSy1s. Therefore, the possibility that the development of relativistic jets in these objects occurs in hosts undergoing strong merger activity, or with non-spiral morphology, cannot be ruled out. Further high-resolution observations of the host galaxies of PMN J0948+0022 and the other γ-ray NLSy1s will be fundamental to obtain insights into the onset of production of relativistic jets in these sources.

7.5 BH mass and jet formation

The mechanism for producing a relativistic jet is still unclear. In particular, the physical parameters that drive the jet formation are still under debate. One of the key parameters should be the BH mass, with only large masses allowing an efficient jet formation (see e.g. Sikora, Stawarz & Lasota 2007). Therefore, one of the most surprising facts related to the discovery of PMN J0948+0022 in gamma-rays was the development of a relativistic jet in an object with a relatively small BH mass, 3.2×10^7 M$_\odot$ (Yuan et al. 2008). Recently, Chiaberge & Marconi (2011) suggested that a BH mass higher than 10^8 M$_\odot$ is necessary for producing a radio-loud AGN and that the merger history together with the subsequent galaxy morphology plays a fundamental role. In any case, the estimated mass of this source, as well as for the other NLSy1s, has large uncertainties. By means of the broad-band SED modelling a BH mass of 1.5×10^8 M$_\odot$ was estimated for PMN J0948+0022 in Foschini et al. (2011). Marconi et al. (2008) suggested that BLR clouds are subjected to radiation pressure from the absorption of ionizing photons, and by applying a correction to the virial relation, we have higher masses for the NLSy1s. Recently, also Calderone et al. (2013) pointed out that the BH masses of the NLSy1s estimated by the modelling of optical/UV data with a Shakura and Sunyaev disc spectrum could be significantly higher than those derived on the basis of single epoch virial methods. In particular, for PMN J0948+0022 they found a value of 10^9 M$_\odot$ in agreement with the typical BH mass of blazars. This may solve the problem of the minimum BH mass predicted in different scenarios of relativistic jet formation and development, but introduces a possible new one. For spiral galaxies, the BH mass typically ranges between 10^6 and 10^8 M$_\odot$ (see e.g. Woo & Urry 2002). If the BH mass is on the larger side of the estimated values, how is it possible to reconcile such a large BH mass with a spiral galaxy?

A second fundamental parameter for the efficiency of relativistic jet production should be the BH spin, with supermassive black holes (SMBH) in elliptical galaxies having on average much larger spins than SMBHs in disc–spiral galaxies, as proposed in the 'modified spin paradigm' (Sikora et al. 2007). This is because the spin evolution of BHs in spiral galaxies seems to be limited by multiple accretion events with random orientation of the angular momentum vectors and small increments of mass, while elliptical galaxies underwent at least one major merger with large matter accretion triggering an efficient spin-up of the SMBHs. Thus, the mass and the spin of the BH seem to be related to the host galaxies, leading to the hypothesis that relativistic jets can efficiently develop only in elliptical galaxy (e.g. Böttcher & Dermer 2002; Marscher 2010). However, the presence of a rapidly spinning BH was inferred by means of X-ray reflection spectroscopy in a few radio-quiet AGNs hosted by spiral/disc galaxies, suggesting that the BH spin is not the only parameter that drives the radio-quiet/radio-loud dichotomy (see e.g. Reynolds 2013).

We noted that BH masses of radio-loud NLSy1s reported in Komossa et al. (2006) and Yuan et al. (2008) are generally larger than those in the entire sample of NLSy1s ($M_{\rm BH} \approx (2\text{–}10) \times 10^7$ M$_\odot$), even if still smaller than those in radio-loud quasars. The larger BH masses of radio-loud NLSy1s could be related to higher mass accretion events that can spin up the BHs. In the same way, the smaller fraction of radio-loud NLSy1s with respect to the radio-loud quasars could be because the high-accretion-rate regime does not last sufficiently long in all NLSy1s to substantially spin up the central BH Sikora (2009).

Another consideration which is likely to be important for jet formation is the nature of the accretion flow. In particular, a geometrically thick accretion flow is needed in order to create large-scale poloidal magnetic fields, which may play a dominant role in the launching of jets (Reynolds, Garofalo & Begelman 2006; Sikora et al. 2013). In cases where standard thin discs are present, the jet activity may be due to the dissipation of coronal magnetic fields (Sikora et al. 2013). For PMN J0948+0022, it is clear that emission from the jet dominates the X-ray spectrum above 2 keV, while we are likely seeing the accretion disc plus corona of the AGN at lower X-ray energies. Although we cannot constrain detailed models for the soft X-ray emission with the current observations, we note that the spectral slope is similar to that found in radio-quiet NLSy1, indicating that a standard disc is present as also expected from the high accretion rate. Future deep X-ray observations with the jet in different states are needed to explore in detail the connection between the disc and jet in this source.

The presence of a relativistic jet in some radio-loud NLSy1 galaxies, first suggested by their variable radio emission and flat spectra, is now confirmed by the *Fermi*-LAT detection of five NLSy1s in γ-rays. PMN J0948+0022 showed all characteristics of the blazar phenomenon with a BH mass of 10^8–10^9 M$_\odot$, not much less than those of blazars. The impact on the γ-ray emission mechanisms of the properties of the central engine in radio-loud NLSy1s, derived from their peculiar optical characteristics, is still under debate. In addition, the detection of relativistic jets in a class of AGN thought to be hosted in spiral galaxies is very intriguing, challenging the theoretical scenario of relativistic jet formation proposed so far. Further, multifrequency observations of this object and other γ-ray-emitting NLSy1s will be fundamental for investigating in detail their characteristics over the entire electromagnetic spectrum.

ACKNOWLEDGEMENTS

The *Fermi* LAT Collaboration acknowledges generous ongoing support from a number of agencies and institutes that have supported both the development and the operation of the LAT as well as scientific data analysis. These include the National Aeronautics and Space Administration and the Department of Energy in the United States, the Commissariat à l'Energie Atomique and the Centre National de la Recherche Scientifique/Institut National de Physique Nucléaire et de Physique des Particules in France, the Agenzia Spaziale Italiana and the Istituto Nazionale di Fisica Nucleare in Italy, the Ministry of Education, Culture, Sports, Science and Technology (MEXT), High Energy Accelerator Research Organization (KEK) and Japan Aerospace Exploration Agency (JAXA) in Japan, and the K. A. Wallenberg Foundation, the Swedish Research Council and the Swedish National Space Board in Sweden. Additional support for science analysis during the operations phase is gratefully acknowledged from the Istituto Nazionale di Astrofisica in Italy and the Centre National d'Études Spatiales in France.

We thank the *Swift* team for making these observations possible, the duty scientists and science planners. The OVRO 40 m monitoring programme is supported in part by NASA grants NNX08AW31G and NNX11A043G, and NSF grants AST-0808050 and AST-1109911. This paper is partly based on observations with the 100 m telescope of the MPIfR (Max-Planck-Institut für Radioastronomie) at Effelsberg and the Medicina telescope operated by INAF-Istituto di Radioastronomia. We acknowledge A. Orlati, S. Righini and the Enhanced Single-dish Control System Development Team. The CSS survey is funded by the National Aeronautics and Space Administration under grant no. NNG05GF22G issued through the Science Mission Directorate Near-Earth Objects Observations Program. The CRTS survey is supported by the US National Science Foundation under grants AST-0909182. This research has made use of observations obtained with the 2.1 m telescope of the Observatorio Astrofisico Guillermo Haro (OAGH), in the state of Sonora, Mexico, operated by the INAOE, Mexico. OAGH acknowledges funding from the INAOE Astrophysics Department. The Metsähovi team acknowledges the support from the Academy of Finland to our observing projects (numbers 212 656, 210 338, 121 148 and others). This research made use of data from MOJAVE data base that is maintained by the MOJAVE team (Lister et al. 2009). This work is based on observations obtained with *XMM–Newton*, an ESA science mission with instrument and contributions directly funded by ESA Member States and the USA (NASA). JL acknowledges financial support from the Swedish National Space Board. FD thanks A. Breeveld and P. Roming for useful discussion about OM and UVOT cross-calibration. JL thanks Andy Fabian for useful discussion. We thank S. Cutini, S. Digel, D. Thompson and the anonymous referee for useful comments and suggestions.

REFERENCES

Abdo A. A. et al., 2009a, ApJ, 699, 976
Abdo A. A. et al., 2009b, ApJ, 707, L142
Abdo A. A. et al., 2009c, ApJ, 707, 727
Abdo A. A. et al., 2010, ApJ, 720, 912
Ackermann M. et al., 2012, ApJ, 747, 104
Angelakis E., Fuhrmann L., Marchili N., Krichbaum T. P., Zensus J. A., 2008, Mem. Soc. Astron. Ital., 79, 1042
Angelakis E. et al., 2013, Proc. Nuclei of Seyfert Galaxies and QSOs - Central Engine and Conditions of Star Formation. preprint (arXiv:1304.1706)
Anton S., Browne I. W. A., Marcha M. J., 2008, A&A, 490, 583
Atwood W. B. et al., 2009, ApJ, 697, 1071
Baars J. W. M., Genzel R., Pauliny-Toth I. I. K., Witzel A., 1977, A&A, 61, 99
Barthelmy S. D. et al., 2005, Space Sci. Rev., 120, 143
Baumgartner W. H., Tueller J., Markwardt C. B., Skinner G. K., Barthelmy S., Mushotzky R. F., Evans P. A., Gehrels N., 2013, ApJS, 207, 19
Bertin E., Arnouts S., 1996, A&AS, 117, 393
Bhattacharyya S., Bhatt H., Bhatt N., Singh K. K., 2013, MNRAS, preprint (arXiv:1301.1150)
Bianchi S., Guainazzi M., Matt G., Fonseca Bonilla N., Ponti G., 2009, A&A, 495, 421
Blandford R. D., Rees M. J., 1978, in Wolfe A. M., ed., BL Lac Objects. Univ. Pittsburgh Press, Pittsburgh, p. 328
Boller T., Bradt W. N., Fink H., 1996, A&A, 305, 53
Böttcher M., Dermer C. D., 2002, ApJ, 564, 86
Burrows D. N. et al., 2005, Space Sci. Rev., 120, 165
Calderone G., Ghisellini G., Colpi M., Dotti M., 2013, MNRAS, 431, 210
Cash W., 1979, ApJ, 228, 939
Celotti A., Ghisellini G., Fabian A. C., 2007, MNRAS, 375, 417
Chiaberge A., Marconi A., 2011, MNRAS, 416, 917
Chitnis V. R., Pendharkar J. K., Bose D., Agrawal V. K., Rao A. R., Misra R., 2009, ApJ, 698, 1207
Crummy J., Fabian A. C., Gallo L., Ross R. R., 2006, MNRAS, 365, 1067
D'Ammando F., Ciprini S., 2011, Astron. Telegram, 3429
D'Ammando F., Orienti M., 2013, Astron. Telegram, 4694
D'Ammando F. et al., 2012a, MNRAS, 426, 317
D'Ammando F. et al. (Fermi-LAT Collaboration), 2012b, AIP Conf. Ser. Vol. 1505, High Energy Gamma-Ray Astronomy: 5th International Meeting on High Energy Gamma-Ray Astronomy. Astron. Soc. Pac., San Francisco, p. 570
D'Ammando F. et al., 2013a, MNRAS, 433, 952
D'Ammando F. et al., 2013b, MNRAS, 436, 191
Deo R. P., Crenshow D. M., Kraemer S. B., 2006, AJ, 132, 321
Djorgovski S. G. et al., 2011, in Mihara T., Kawai N., eds, The First Year of MAXI: Monitoring Variable X-ray Sources. JAXA Special Publ., Tokyo, preprint (arXiv:1102.5004)
Doi A., Nagai H., Asada K., Kameno S., Wajima K., Inoue M., 2006, PASJ, 58, 829
Donato D., Ghisellini G., Tagliaferri G., Fossati G., 2001, A&A, 375, 739
Done C., Davis S. W., Jin C., Blaes O., Ward M., 2012, MNRAS, 420, 1848
Drake A. J. et al., 2009, ApJ, 696, 870
Eggen J. R., Miller H. R., Maune J. D., 2013, ApJ, 773, 85
Foschini L., Maraschi L., Tavecchio F., Ghisellini G., Gliozzi M., Sambruna R. M., 2009, Adv. Space Res., 43, 889
Foschini L. et al., 2011, MNRAS, 413, 1671
Foschini L. et al., 2012, A&A, 548, 106
Fuhrmann L., Zensus J. A., Krichbaum T. P., Angelakis E., Readhead A. C. S., 2007, in Ritz S., Michelson P., Meegan C. A., eds, AIP Conf. Ser. Vol. 921, The First GLAST Symposium. Am. Int. Phys., New York, p. 249
Fuhrmann L. et al., 2008, A&A, 490, 1019
Gallo L. C. et al., 2006, MNRAS, 370, 245
Gehrels N. et al., 2004, ApJ, 611, 1005
Gierliński M., Done C., 2004, MNRAS, 349, L7
Giroletti M. et al., 2011, A&A, 528, L11
Gliozzi M., Sambruna R. M., Jung I., Krawczynski H., Horan D., Tavecchio F., 2006, ApJ, 646, 61
Grupe D., Komossa S., Leighly K. M., Page K. L., 2010, ApJS, 187, 64
Itoh R. et al., 2013, ApJ, 775, L26
Jansen F. et al., 2001, A&A, 365, L1
Kalberla P. M. W., Burton W. M., Hartmann D., Arnal E. M., Bajaja E., Morras R., Pöppel W. G. L., 2005, A&A, 440, 775
Kataoka J. et al., 2008, ApJ, 672, 787
Komossa S., Voges W., Xu D., Mathur S., Adorf H.-M., Lemson G., Duschi W. J., Grupe D., 2006, AJ, 132, 531
Landau R. et al., 1986, ApJ, 308, 78
Larsson J., Miniutti G., Fabian A. C., Miller J. M., Reynolds C. S., Ponti G., 2008, MNRAS, 384, 1316

Lister M. L. et al., 2009, AJ, 137, 3718
Liu H., Wang J., Mao Y., Wei J., 2010, ApJ, 715, L113
Lucarelli F. et al., 2011, Astron. Telegram, 3448
Marconi A., Axon D., Maiolino R., Nagao T., Pastorini G., Pietrini P., Robinson A., Torricelli G., 2008, ApJ, 678, 693
Markowitz A., Edelson R., 2004, ApJ, 617, 939
Marscher A., 2010, in Belloni T., ed., Lecture Notes in Physics 794, The Jet Paradigm. Springer, Berlin, p. 173
Marscher A. P., 2012, 2011 Fermi Symposium Proceedings - eConf C110509 preprint (arXiv:1201.5402)
Mason K. O. et al., 2001, A&A, 365, L36
Massaro E., Perri M., Giommi P., Nesci R., 2004, A&A, 413, 489
Mattox J. R. et al., 1996, ApJ, 461, 396
Maune J. D., Miller H. R., Eggen J. R., 2011, in Foschini L., Colpi M., Grupe D., Komossa S., Leighly K., Mathur S., eds, Proc. Sci., Narrow-Line Seyfert 1 Galaxies and their Place in the Universe. SISSA, Trieste
Maune J. D., Miller H. R., Eggen J. R., 2013, ApJ, 762, 124
Nemmen R. S., Georganopoulos M., Guiriec S., Meyer E. T., Gehrels N., Sambruna R. M., 2012, Science, 338, 1445
Nolan P. et al., 2012, ApJS, 199, 31
Osterbrock D. E., Pogge R. W., 1985, ApJ, 297, 166
Paliya V. S., Stalin C. S., Kumar B., Kumar B., Bratt V. K., Pandey S. B., Yadav R. K. S., 2013, MNRAS, 428, 2450
Ponti G., Cappi M., Czerny B., Goosmann R. W., Karas V., 2007, in Karas V., Matt G., eds, IAU Symp. 238, Black Holes from Stars to Galaxies – Across the Range of Masses. Cambridge Univ. Press, Cambridge, p. 429
Raiteri C. M. et al., 2010, A&A, 524, 43
Raiteri C. M. et al., 2011, A&A, 534, 87
Ravasio M., Tagliaferri G., Ghisellini G., Tavecchio F., 2004, A&A, 424, 841
Reynolds C. S., 2013, Space Sci. Rev., preprint (arXiv:1302.3260)
Reynolds C. S., Garofalo D., Begelman M. C., 2006, ApJ, 651, 1023
Richards J. L. et al., 2011, ApJS, 194, 29
Roming P. W. A. et al., 2005, Space Sci. Rev., 120, 95
Ross R. R., Fabian A. C., 2005, MNRAS, 358, 211
Shakura N. I., Sunyaev R. A., 1973, A&A, 24, 337
Sikora M., 2009, Astron. Nachr., 330, 291
Sikora M., Begelman M. C., 2013, ApJ, 764, L24
Sikora M., Stawarz L., Lasota J.-P., 2007, ApJ, 658, 815
Teräsranta H. et al., 1998, A&AS, 132, 305
Titarchuk L., 1994, ApJ, 434, 570
Vaughan S., Edelson R., Warwick R. S., Uttley P., 2003, MNRAS, 345, 1271
Wilms J., Allen A., McCray R., 2000, ApJ, 542, 914
Woo J.-H., Urry C. M., 2002, ApJ, 579, 530
Yuan W., Zhou H.-Y., Komossa S., Dong X.-B., Wang T.-G., Lu H. L., Bai J. M., 2008, ApJ, 685, 801
Zhou H.-Y., Zhang S.-N., 2010, ApJ, 713, 11
Zhou H.-Y., Wang T.-G., Dong X.-B., Zhou Y.-Y., Li C., 2003, ApJ, 584, 147
Zhou H.-Y., Wang T.-G., Yuan W., Lu H. L., Dong X.-B., Wang J., Lu Y., 2006, ApJS, 166, 128
Zhou H.-Y. et al., 2007, ApJ, 658, L13

This paper has been typeset from a TEX/LATEX file prepared by the author.